Title

Precise Tuning of Surface Quenching for Luminescence Enhancement in Core—Shell Lanthanide-Doped Nanocrystals

Journal

Nano Letters, 16(11)

ISSN

1530-6984

Authors

Fischer, Stefan

Bronstein, Noah D

Swabeck, Joseph K

et al.

Publication Date

2016-11-09

DOI

10.1021/acs.nanolett.6b03683

Peer reviewed

NANO LETTERS

Letter

pubs.acs.org/NanoLett

Precise Tuning of Surface Quenching for Luminescence Enhancement in Core−Shell Lanthanide-Doped Nanocrystals

Stefan Fischer,[†,‡] Noah D. Bronstein,[†,‡] Joseph K. Swabeck,[†,‡] Emory M. Chan,[§] and A. Paul Alivisatos*[,†,‡,∥,⊥]

[†]Materials Sciences Division, Lawrence Berkeley National Laboratory, Berkeley, California 94720, United States

[‡]Department of Chemistry, University of California—Berkeley, Berkeley, California 94720, United States

[§]Molecular Foundry, Lawrence Berkeley National Laboratory, Berkeley, California 94720, United States

[∥]Department of Materials Science and Engineering, University of California—Berkeley, Berkeley, California 94720, United States

[⊥]Kavli Energy NanoScience Institute, Berkeley, California 94720, United States

Supporting Information

ABSTRACT: Lanthanide-doped nanocrystals are of particular interest for the research community not only due to their ability to shape light by downshifting, quantum cutting, and upconversion but also because novel optical properties can be found by the precise engineering of core−shell nanocrystals. Because of the large surface area-to-volume ratio of nanocrystals, the luminescence is typically suppressed by surface quenching. Here, we demonstrate a mechanism that exploits surface quenching processes to improve the luminescence of our core−shell lanthanide-doped nanocrystals. By carefully tuning the shell thickness of inert β-$NaLuF_4$ around β-$NaYF_4$ nanocrystals doped with Yb^{3+} and Er^{3+}, we unravel the relationship between quantum yield and shell thickness, and quantify surface quenching rates for the relevant Er^{3+} and Yb^{3+} energy levels. This enhanced understanding of the system's dynamics allowed us to design nanocrystals with a surface quenching-assisted mechanism for bright NIR to NIR downshifting with a distinctive efficiency peak for an optimized shell thickness.

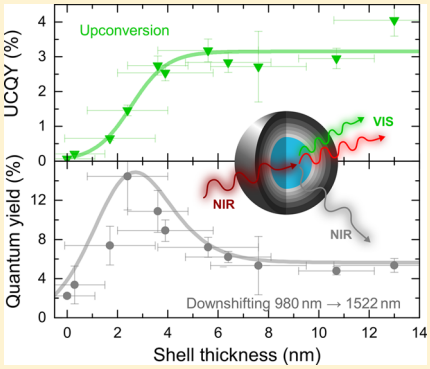

KEYWORDS: *Upconversion, downshifting, lanthanide, core−shell, nanocrystals, surface quenching, quantum yield, NIR, photoluminescence*

Lanthanide ions (Ln) are widely used in optical and photonic applications due to their unique photophysical properties. The manifold 4*f* energy level structure of the trivalent Ln results in a great amount of combinatorial diversity, enabling systems like the most efficient downshifting phosphors for white LEDs[1,2] as well as downconverting (quantum cutting) and upconverting materials for enhanced solar cell performance,[3−5] for example. Lanthanide-doped nanocrystals receive great attention not only due to their promising potential in life sciences,[6−8] solar energy harvesting,[3,5,9] or as safety markers[10,11] but also because of their novel properties due to nanoengineering which, for example, allows designing of energy transfer schemes[12,13] or nonsteady state upconversion for full-color luminescence in a single nanocrystal.[14] However, the promising potential and applicability of lanthanide-doped nanocrystals is often limited by the low luminescence efficiency due to the large surface area to volume ratio of the nanocrystals combined with the competition between the typically slow radiative processes and more rapid surface-related nonradiative quenching processes.[5,15] For example, the upconversion quantum yield (UCQY) of micro- or monocrystalline materials, also referred to as bulk, is typically 100 to 10 000 times higher than the UCQY of their nanomaterial counterparts under the same experimental conditions.[5,15,16]

Growth of an inert shell around the optically active nanocrystal core is a commonly used strategy to reduce surface quenching processes, which leads to a significantly increased quantum yield.[15,16] Although great advances have been achieved over the past few years leading to Er^{3+}-doped core−shell upconverting nanocrystals reaching up to one-sixth of the bulk value,[9] there is still a significant efficiency discrepancy of ∼26 times between bulk material and nanocrystals for one of the most studied upconverting materials, hexagonal-phase (β-)$NaYF_4$ doped with Yb^{3+} and Er^{3+}.[5,15,17,18] Here, we investigate the role of surface quenching processes on the optical properties of β-$NaYF_4$ doped with Yb^{3+} and Er^{3+} as a function of the β-$NaLuF_4$ shell thickness. We demonstrate that understanding of surface-related nonradiative quenching processes not only allows engineering of more efficient and brighter nanocrystals but also enables the design of surface quenching-assisted luminescence pathways.

Received: September 1, 2016
Revised: October 6, 2016
Published: October 11, 2016

DOI: 10.1021/acs.nanolett.6b03683
Nano Lett. 2016, 16, 7241−7247

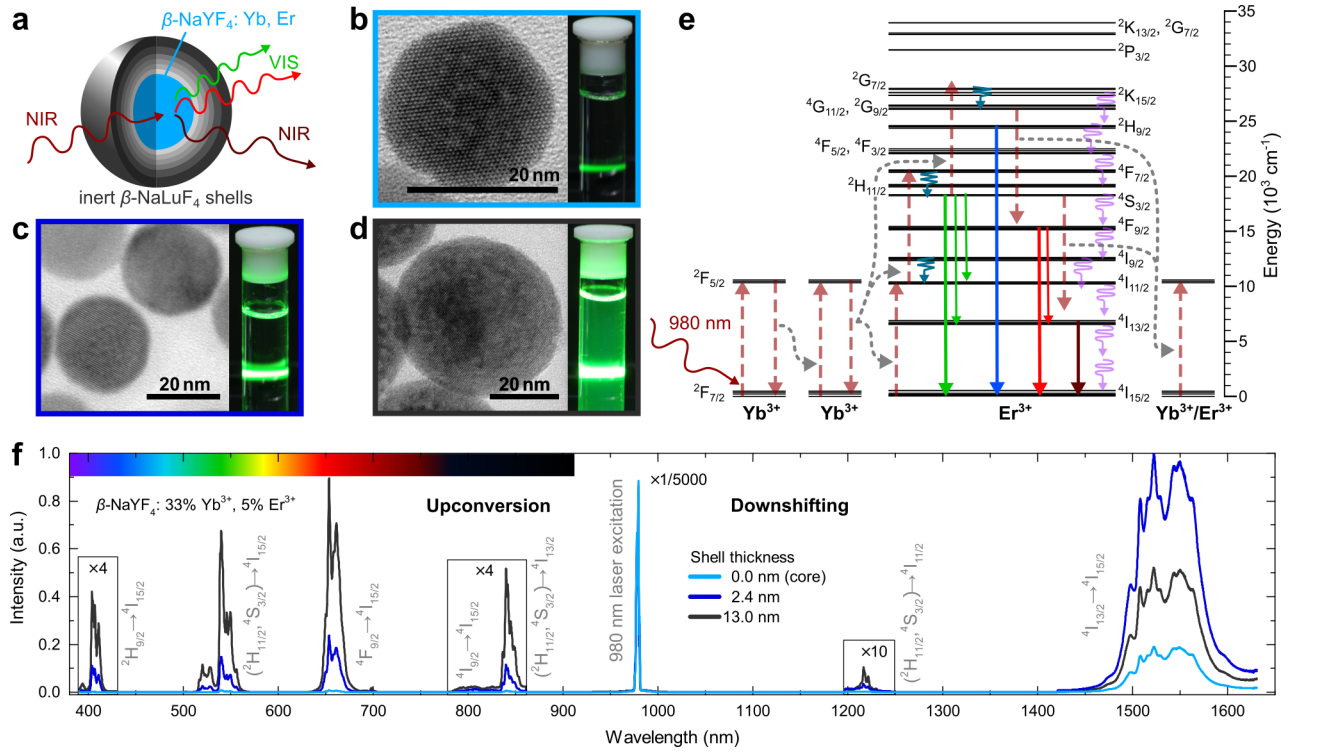

Figure 1. Efficient visible upconversion and near-infrared downshifting in β-$NaYF_4$: Yb^{3+}, Er^{3+}@$NaLuF_4$ core–shell nanocrystals. (a) Design of core–shell particles using the same β-$NaYF_4$: Yb^{3+}, Er^{3+} core but different β-$NaLuF_4$ shell thicknesses. (b–d) TEM images of the β-$NaYF_4$: Yb^{3+}, Er^{3+} core as well as core–shell nanocrystals with a 2.4 and 13.0 nm thick β-$NaLuF_4$ shell, respectively. All scale bars are 20 nm. The photographs show the bright visible upconversion under 980 nm laser excitation with 63 W/cm^2. (e) Schematic representation of the upconversion and downshifting process under 980 nm excitation. The incident photons are predominantly absorbed by Yb^{3+} and the energy is transferred to Er^{3+}. However, the excitation energy migrates through the entire core nanocrystal by efficient hopping from one Yb^{3+} ion to another neighboring Yb^{3+}. (f) Emission spectrum of bright upconversion at shorter wavelengths and simultaneously strong NIR downshifting luminescence from $Er^{3+4}I_{13/2}$ energy level for the three samples shown in panels b–d.

In our approach, we chose β-$NaYF_4$ doped with Yb^{3+} and Er^{3+} because it is known for its high efficiency of converting near-infrared (NIR) 980 nm photons to visible (green and red) light[3,5,15,16] (Figure 1a). We synthesized a large amount of monodisperse and nearly spherical β-$NaYF_4$: 33% Yb^{3+}, 5% Er^{3+} nanocrystals with an average diameter of 23.8 ± 1.2 nm (Figure 1b). Isotropic β-$NaLuF_4$ shells were grown around the core nanocrystals with shell thicknesses from 0.3 to 13.0 nm (Supporting Information, Materials). The inert nature of these shells is evident by the increase in the brightness of upconverted photons when the shell is present, which is immediately apparent to the eye (Figure 1b–d).

In our system, Yb^{3+} act as sensitizers for Er^{3+}. The excitation energy is transferred multiple times from one Yb^{3+} to another before it reaches a neighboring Er^{3+} in the crystal lattice where it then transfers the excitation energy to the Er^{3+} via dipole–dipole energy transfer (ET). Because dipole–dipole ET scales with the distance between donor and acceptor with $1/d^6$, dipole–dipole ET is most efficient between the closest neighbors in the lattice. Once an Er^{3+} is in an excited state, it can be pumped into higher excited states by additional dipole–dipole ET processes from excited Yb^{3+} at neighboring lattice sites (Figure 1e). In this upconversion scheme, the Er^{3+} energy level $^4F_{9/2}$ with red luminescence may require three photons to be excited, whereas the energetically higher $^2S_{3/2}$ energy level with green luminescence only requires two photons[18] (Supporting Information, Excitation Spectra). Here, we would like to note that the system is dynamic with multiple processes occurring simultaneously. There is also an ongoing discussion in the literature whether the population of the Er^{3+} $^4F_{9/2}$ energy level is a two- or three-photon process.[18] Most likely, there are different processes populating the Er^{3+} $^4F_{9/2}$ energy level with two- or three-photon absorption characteristics. One example for a two-photon process would be the population of $^4I_{13/2}$ followed by energy transfer from the Yb^{3+} $^2F_{5/2} \rightarrow {}^2F_{7/2}$ to the Er^{3+} $^4I_{13/2} \rightarrow {}^4F_{9/2}$. Besides the bright upconversion luminescence from these levels, we also found a strong NIR downshifted emission from the Er^{3+} energy level $^4I_{13/2}$ between 1500 and 1600 nm (Figure 1f).[19] This luminescence arises through a complex series of events and is one that can be manipulated in interesting and unexpected ways by variation of the shell thickness, as discussed below.

We measured time-dependent luminescence, excitation spectra, and quantum yield as a function of the irradiance for the core and all 10 core–shell samples to understand our system in detail and all the dependencies between shell thickness and surface quenching (Supporting Information, Optical Characterization). The UCQY of our core upconverting nanocrystals is 0.07% under 980 nm laser excitation at 63 W/cm^2 with a red-to-green ratio of 1.5, which is very similar to reported values in literature.[15] The UCQY increases with the shell thickness, as expected, due to a reduction in surface quenching losses. The highest reported UCQY values in literature for comparable experiments using a bulk upconverter are 7.5% at 35 W/cm^2 by modeling[18] and 7.8 ± 1.2% at 22 W/cm^2 experimentally.[17,5] Here, we measured an UCQY value

DOI: 10.1021/acs.nanolett.6b03683
Nano Lett. 2016, 16, 7241–7247

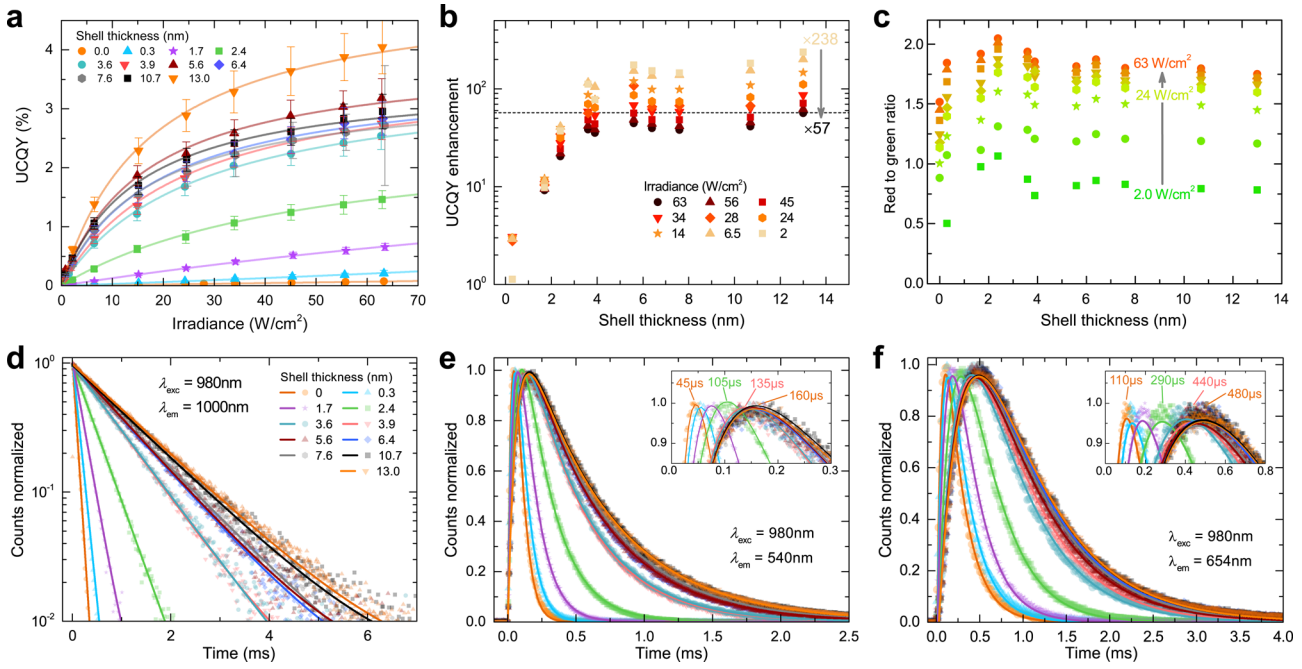

Figure 2. Power-dependent UCQY and time-dependent photoluminescence measurements of the β-$NaYF_4$: Yb^{3+}, Er^{3+} nanocrystals as a function of the β-$NaLuF_4$ shell thickness. (a) The UCQY of the upconversion luminescence increases with shell thickness as well as irradiance of the continuous-wave 980 nm laser. Here, the sum of emissions from the Er^{3+} $^2S_{3/2}$, $^4H_{11/2}$ (green) and $^4F_{9/2}$ (red) energy levels are shown. The lines are empirical fits. (b) Enhancement factor of the UCQY increases rapidly with inert shell thickness but appears to saturate at shell thicknesses above 4 nm. At a low irradiance of 2 W/cm^2, the UCQY of the best core−shell nanocrystals is 238 times larger than the value obtained for the bare core upconverting nanocrystal at the same excitation conditions. The more pronounced bending of the UCQY curve of the core−shell nanocrystals in (a) results in lower enhancement factors at higher irradiances. (c) The upconversion emission of the Er^{3+} $^4F_{9/2}$ (red) energy level increases significantly with increasing irradiance, as expected for a three-photon process compared to the two-photon process to populate the Er^{3+} $^2S_{3/2}$, $^4H_{11/2}$ (green) energy levels. (d) Time-dependent Yb^{3+} $^2F_{5/2}$ emission after 980 nm excitation (pulse energy density ~0.02 mJ/mm^2) for the nanocrystals as a function of the inert shell thickness. The intrinsic lifetime of the Yb^{3+} $^2F_{5/2}$ energy level is enhanced by a factor of 16 due to reduced surface quenching from the 13.0 nm thick shell. (e,f) Time-dependent upconversion luminescence of the Er^{3+} $^4S_{3/2}$ and $^4F_{9/2}$ energy levels after 980 nm excitation, respectively. With increasing shell thickness, the decay lifetime as well as the rise time lengthens, demonstrating efficient passivation of the surface quenching processes. A vial-type function, which is a combination of two exponential function with contrary algebraic signs, was fitted to the time-dependent upconversion luminescence.

of 4.0 ± 0.5% at 63 W/cm^2 for our upconverting nanocrystals with a 13 nm thick β-$NaLuF_4$ shell (Figure 2a), which is 57 times more efficient than the unshelled core nanocrystal. Although this is a great step forward toward the most efficient Yb^{3+}, Er^{3+}-doped upconverter material, it is still only half the UCQY value of the bulk material. We did not observe significant enhancement in the efficiency for shell thicknesses above 4−5 nm, and the enhancement factor, which is the ratio of UCQY from core−shell to core nanocrystals, saturates at larger shell thicknesses (Figure 2b). The enhancement factor also decreases for higher irradiances as a direct result of saturation effects and a consequently more pronounced bending of the UCQY curves for thicker shells (see Figure 2a). We also observed higher red-to-green ratio of the UC luminescence for higher excitation power, which reflects the higher characteristic power dependence of the three-photon upconversion red emission compared to the two-photon green emission (Figure 2c). The comparatively high red-to-green ratio is a result of energy transfer processes between Er^{3+} ions due to the high Er^{3+} doping of 5% in contrast to the commonly used 2%. As mentioned before, energy transfer from Yb^{3+} $^2F_{5/2}$ → $^2F_{7/2}$ to Er^{3+} $^4I_{13/2}$ → $^4F_{9/2}$ populates the red-emitting Er^{3+} $^4F_{9/2}$ energy level. The probability of this energy transfer process increases with the occupation of the Er^{3+} $^4I_{13/2}$ energy level. Interestingly, the peak of the red-to-green ratio for a shell thickness of 2.4 nm corresponds to a peak in the occupation of the Er^{3+} $^4I_{13/2}$ energy level. The special role of the Er^{3+} $^4I_{13/2}$ energy level will be discussed later. In conclusion, our results suggest that the most efficient core−shell upconverting nanocrystals are not limited by surface quenching but more likely by volume effects in the nanocrystal, such as crystal defects, doping level, or distribution of dopants.

To understand the photophysical dynamics of the system, we next measured the time-dependence of the core−shell nanocrystal luminescence. The lifetime of the Yb^{3+} $^2F_{5/2}$ energy level increases continuously with shell thickness because nonradiative surface quenching processes are passivated more and more effectively (Figure 2d). As a consequence, there is more time for the excitation energy to migrate through the nanocrystal, increasing the probability of ET to an Er^{3+}. Because of this, the onset of the green and red upconversion luminescence shifts to 4 times longer times for >4 nm thick shells (Figure 2e,f), reaching onset times of nearly half of a millisecond for the red emission and 160 μs for the green emission. The decay time of green and red luminescence increases significantly with shell thickness, which is also the case when the corresponding Er^{3+} energy levels are excited directly (Supporting Information Figures S16 and S17).

Next, we used the Yb^{3+} decay time τ_{Yb}, which we obtained from monoexponential fitting, to determine the surface quenching rate of the Yb^{3+} $^2F_{5/2}$ energy level. Here, we would like to note that in this nonlinear system the lifetime of

DOI: 10.1021/acs.nanolett.6b03683
Nano Lett. 2016, 16, 7241−7247

the energy levels may depend on the pulse energy density (irradiance) of the excitation, which was in our case 0.02 mJ/mm^2 for 980 nm excitation with a repetition rate of 20 Hz. To justify our assumptions on surface quenching, we first modeled the energy migration in β-$NaYF_4$: Yb^{3+}, Er^{3+} material systems, based on an analytical model[9] (Supporting Information, Migration Modeling). In our case, we determined an average migration path length in a three-dimensional random walk model of roughly 28 nm, which is almost 2.5 times larger than the radius of our core nanocrystals. Hence, it is reasonable to assume surface quenching to be a nonradiative process which influences all the Yb^{3+} ions in the nanocrystal, whether they are close to the surface or in the center of the nanocrystal because the excitation energy migrates throughout the entire nanocrystal.

In our surface quenching model, we define the measured decay time τ_{Yb} as a combination of the intrinsic lifetime $\tau_{intrinsic}$ of the Yb^{3+} $^2F_{5/2}$ energy level, which is constant for all shell thicknesses (d_{shell}), and a nonradiative surface quenching decay time τ_{SQ} with corresponding surface quenching rate Γ_{SQ}, which explicitly depends on d_{shell}

$$\frac{1}{\tau(d_{shell})} = \frac{1}{\tau_{intrinsic}} + \frac{1}{\tau_{SQ}(d_{shell})} = \frac{1}{\tau_{intrinsic}} + \Gamma_{SQ}(d_{shell}) \quad (1)$$

We then used this equation and fitted an exponential surface quenching model with

$$\Gamma_{SQ} = \Gamma_0 \exp(-\kappa d_{shell}) \left(\frac{R_{core} + d_{shell}}{R_{core}} \right)^2 \quad (2)$$

to the Yb^{3+} decay times (Figure 3a). In this surface quenching model, Γ_0 is the surface quenching rate without shell, κ defines the exponential passivation improvement with shell thickness, and the last term addresses the increasing surface area as the shell becomes thicker. The exponential model was motivated by the tunneling probability through a potential barrier, such as the Marcus–Levich–Jortner equation for acceptor–donor distance dependence on electron transfer rates.[20] We also tested other surface quenching models but the exponential approach fit best to the Yb^{3+} decay times (Supporting Information, Surface Quenching Analysis). The exponential surface quenching model also fits the UCQY as a function of shell thickness very well (inset Figure 3b). This result suggests that within a series of upconverting nanocrystals (e.g., studying the effect of different ligands or solvents), the lifetime measurement of the Yb^{3+} $^2F_{5/2}$ energy level may be a sufficient indicator of the UCQY for that study, which would significantly ease quantification of such experiments due to the issues of availability and error susceptibility of UCQY measurements.

To investigate the power dependence of the UCQY further, we used the derivative of the fitted curves to determine the critical shell thickness where half the maximum UCQY value is obtained (Figure 3b). For increasing irradiance, thinner shells are required to reach half the maximum UCQY. We interpret this shift to smaller shell thicknesses as a saturation effect of surface quenching, similar to what is reported for small upconverting nanocrystals with high doping levels in the literature.[21] At higher excitation powers, more Yb^{3+} are excited and more excitations migrate through the crystal. The surface quenching rate competes with all the other processes and cannot quench all the excited states of the lanthanide ions that

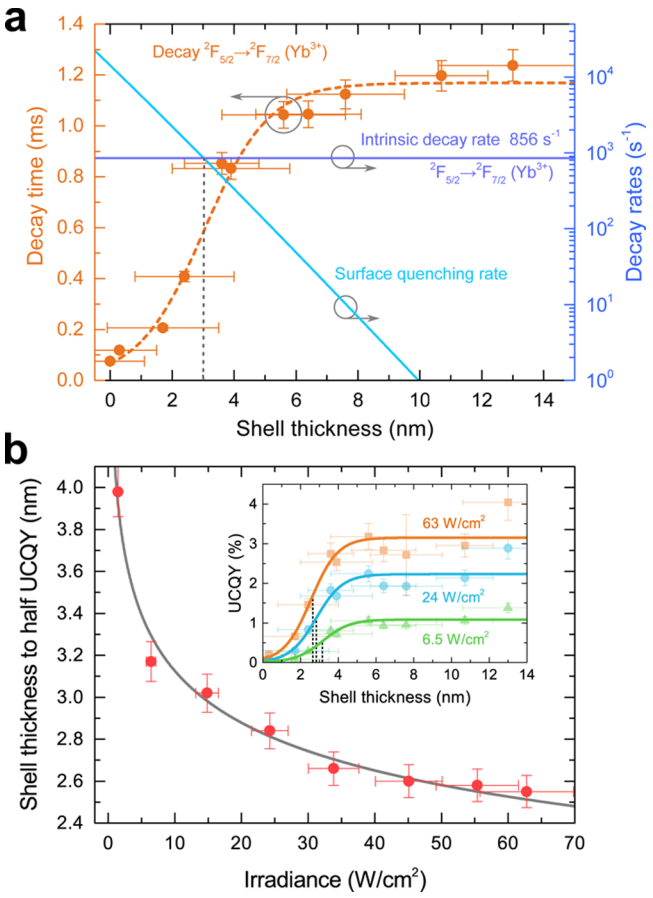

Figure 3. Determination of the surface quenching rates. (a) The decay time of the Yb^{3+} $^2F_{5/2}$ emission from Figure 2a was fitted with our surface quenching model (eqs 1 and 2) to extract the surface quenching parameters Γ_0 and κ as well as the intrinsic lifetime of the $^2F_{5/2}$ energy level. (b) The surface quenching model also reproduces the shell thickness-dependent UCQY measurements (inset). The shell thickness to reach half the maximum UCQY value decreases significantly with the irradiance, revealing that the UCQY limiting process in core–shell nanocrystals at high irradiances is not likely to be surface quenching but rather a rate-limiting step in the upconversion scheme itself.

are reaching the surface at higher generation rates from higher excitation powers.

In addition to the Yb^{3+} $^2F_{5/2}$ energy level, we also used the same model to determine the surface quenching rates for the Er^{3+} energy levels. We found different parameters Γ_0 and κ for the different energy levels (Supporting Information Table S5). In our understanding, surface quenching is a nonradiative process that mainly transfers an excited energy level of a lanthanide ion into an energetically lower lying energy level, similar to multiphonon relaxation. The probability of multiphonon relaxation processes typically decreases exponentially with the number of phonons required to bridge the energy gap between the energy levels, which is known as the energy gap law.[22,23] Here, we assume a very similar dependence for the surface quenching rate due to vibrational modes in the organic molecules adsorbed on the surface, such as the methylene (CH_2) C–H stretch modes in the long alkane chain of oleic acid at ~2900 cm^{-1}, which is close to the energy gap of ~3500 cm^{-1} between the $^4I_{11/2}$ and $^4I_{13/2}$ Er^{3+} energy levels.[24] Because of this, it is not surprising to find different surface quenching parameters Γ_0 and κ for different energy levels that have

DOI: 10.1021/acs.nanolett.6b03683
Nano Lett. 2016, 16, 7241–7247

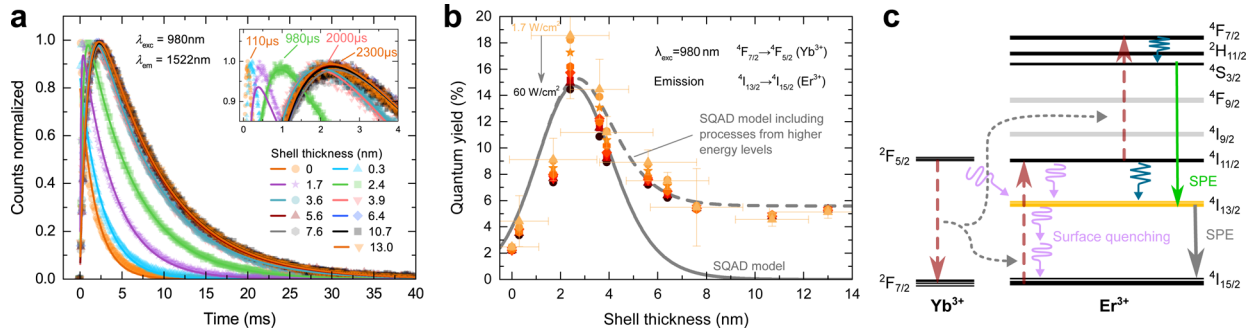

Figure 4. Downshifting luminescence from the Er^{3+} $^4I_{13/2}$ energy level at 1522 nm. (a) The time-dependent downshifting luminescence under 980 nm excitation shows long delays between the laser pulse and the apex of up to 2300 μs. Such long rise times can only be explained by a series of energy transfer processes to populate the $^4I_{13/2}$ energy level. On the other hand, the shorter rise times suggest that surface quenching plays a vital role for thinner shells. (b) The distinctive peak of the NIR to NIR downshifting quantum yield for a shell thickness of 2.4 nm is a result of competing surface quenching processes, which are populating and depopulating the Er^{3+} $^4I_{13/2}$ energy level. This is in very good agreement with a SQAD model based on the surface quenching rates determined in our study. (c) Schematic representation detailing the SQAD model. For thicker shells, surface quenching processes to populate the Er^{3+} $^4I_{13/2}$ energy level are suppressed and energetically higher energy levels become more relevant to populate $^4I_{13/2}$, such as spontaneous emission and energy transfer processes between Er^{3+}.

different energy gaps to be bridged. In contrast to multiphonon relaxation, however, surface quenching processes are not only attenuated by larger energy gaps but also by spatially separating the quenchers on the surface from the lanthanide ions by an inert shell, as described by eq 2.

The dependence of the surface quenching rate on the energy gap between the involved energy levels and the shell thickness can be exploited usefully for the emission from the $^4I_{13/2}$ Er^{3+} energy level. We measured efficient NIR to NIR downshifting luminescence from the $^4I_{13/2}$ Er^{3+} energy level around 1500 to 1600 nm under excitation of the $^2F_{5/2}$ Yb^{3+} energy level at 980 nm. Looking at the $^4I_{13/2}$ Er^{3+} energy level, there are only a few major depopulation processes, namely spontaneous emission, excited state absorption, ET, and nonradiative processes such as multiphonon relaxation or surface quenching. Surface quenching is the only process that directly depends on the shell thickness.

Time-dependent measurements using 980 nm light revealed strongly increasing rise times of the downshifting luminescence with increasing shell thickness (Figure 4a). The apex of the time-dependent emission measurements for the core−shell nanocrystals is up to 20 times longer than the delay for the nanocrystals without shells. The very long delays for shell thicknesses above 4 nm is a strong indicator that several ET processes are involved to populate the $^4I_{13/2}$ energy level. In contrast, the much shorter delay for thin shells suggests a more direct population of the $^4I_{13/2}$ Er^{3+} energy level, which is typically a faster process than the population via ET between several energy levels. Surface quenching can transfer energy of the $^4I_{11/2}$ Er^{3+} or the $^4F_{5/2}$ Yb^{3+} energy level to the $^4I_{13/2}$ energy level by exciting one CH_2 vibrational mode in the oleic acid ligand, for example.[24] On the other hand, to depopulate the $^4I_{13/2}$ Er^{3+} energy level more than two of these vibrational modes need to be excited to bridge the ~6500 cm^{-1} energy gap to the ground level $^4I_{15/2}$, which is much less likely. This is also reflected in the 47 times lower surface quenching rate to depopulate the $^4I_{13/2}$ Er^{3+} energy level compared to the one depopulating the $^4I_{11/2}$ Er^{3+} energy level (Supporting Information Table S5). As a result of the competing processes, we determined a distinct peak in the NIR to NIR downshifting quantum yield at a shell thickness of 2.4 nm (Figure 4b).

We modeled the NIR downshifting luminescence as a function of the shell thickness using a simplified rate equation model considering the previously determined surface quenching rates as well as the intrinsic decay rates (Figure 4c). We found a very good agreement with our experimental data (Figure 4b and Supporting Information, SQAD Model). This demonstrates that surface quenching can be a beneficial nonradiative process, whereas it is usually considered to be a loss mechanism that needs to be avoided. In our case, surface quenching processes are exploited to increase an energy level's population, which consequently leads to brighter luminescence from this energy level. As a result, the quantum yield value of the NIR to NIR luminescence due to surface quenching-assisted downshifting (SQAD) in thin shelled nanocrystals is considerably higher compared to the case where surface quenching is mainly suppressed for very thick shells.

The concept of SQAD is interesting for applications in life sciences and is also applicable in aqueous environments, as vibrational modes in H_2O are in a useful range around 3500 cm^{-1}.[25,26] The properties of NIR to NIR downshifting in our core−shell nanocrystals are beneficial for bioimaging: high quantum yield (fairly constant with excitation power), deep tissue penetration of the 980 nm excitation, emission between 1500 and 1600 nm in the third optical window, and delay between excitation pulse and emission peak of more than 1 ms. The large delay time effectively enhances the signal-to-noise ratio in time-delayed detection as the tissue's self-luminescence decays orders of magnitude faster and therefore does not perturb the imaging of the nanoparticle's luminescence. Additionally, scattering of 1500 to 1600 nm photons in brain and breast tissue is reduced by factors of 3 and 2 compared to 540 and 980 nm photons, respectively.[27] This increases the intrinsic resolution of tissue imaging significantly. Additionally, our nanocrystals showed bright upconversion luminescence at high excitation powers. Therefore, a possible application of our nanocrystals could be in theranostics, that is, imaging of the nanocrystals by NIR to NIR downshifting at low lasers powers and photoinitiated drug release in the vicinity of the nanocrystal at higher excitation powers due to upconverted photons, for example.

In conclusion, we demonstrated a mechanism that exploits surface quenching processes to enhance downshifting luminescence of β-$NaYF_4$: Yb^{3+}, Er^{3+} core−shell nanocrystals, whereas

DOI: 10.1021/acs.nanolett.6b03683
Nano Lett. 2016, 16, 7241−7247

surface quenching is commonly understood as a loss mechanism. The quantum yield of the 1530 nm luminescence under 980 nm excitation is considerably enhanced due to SQAD. We modeled the SQAD process using surface quenching rates, which were determined using time-dependent measurements of the luminescence from individual energy levels. In addition, upconversion quantum yield values up to 4.0 ± 0.5% were measured under 980 nm excitation at 63 W/cm^2. It is likely that future work optimizing the dopant density would significantly improve the luminescence efficiency beyond the values reported here, unless the nanocrystals are limited by some other loss pathway such as crystal defects or poor dopant distribution caused by the significantly lower fabrication temperature compared to the bulk materials.

SQAD is only observable in nanomaterials due to the large surface area to volume ratio required for considerable surface quenching rates. The concept of surface quenching assisted luminescence can be applied to many other lanthanide-doped nanocrystals and is a promising luminescent platform in media where typically surface quenching is considered to be a limitation and not an opportunity to improve optical properties.

Methods. *Synthesis of Core and Core–Shell Nanocrystals.* The β-$NaYF_4$: Yb^{3+}, Er^{3+} core nanocrystals were synthesized following a solvent-thermal literature method with slight modifications.[28,29] The sequential injection shelling procedure of liquid shell precursor into the hot reaction vessel was developed based on the methods presented in refs 29 and 30. All nanocrystals were analyzed by transmission electron microscopy (TEM), X-ray diffraction (XRD), and inductive coupled plasma atomic emission spectroscopy. Further experimental details are provided in the Supporting Information, Materials.

Spectroscopy. Excitation spectra and time-dependent measurements were performed with a FLS980 fluorescence spectrometer from Edinburgh Instruments. A 450 W Xe-lamp and a monochromator were used to conduct excitation spectra experiments. We used an Opotek Nd:YAG laser driven optical parametric oscillator (OPO) Opolette HE 350 LD as excitation source in all time-dependent measurements. The lifetime data was obtained with multichannel scaling (MCS) method. Further experimental details are provided in the Supporting Information, Optical Characterization.

Quantum Yield Measurements. The custom-built quantum yield setup consisting of a 4-port integrating sphere (Labsphere Inc.) with an inner diameter of 5.3 in. with Spectralon coating and a Princeton Instruments SP2300 spectrometer equipped with a Si charge-coupled device (CCD) camera (Princeton Instrument, PIXIS 400B) and an indium gallium arsenide (InGaAs) CCD camera (Andor, iDus InGaAs 1.7 μm). A 2 W continuous-wave 980 nm laser (CNI, MDL-III-980) with power stability <0.185% over 4 h was used as excitation source. The beam area at the sample position of 2.0 ± 0.1 mm^2 was measured with a beam profiler (DataRay, WinCamD-UCD12-1310). The laser power was continuously monitored with a thermal power sensor (S401C, Thorlabs) and the detected spectra corrected for power fluctuation between multiple measurements. The laser power incident on the sample was attenuated using optical density filters in the laser beam path. The complete system was calibrated with a NIST-traceable radiometric calibration source (OceanOptics, HL-CAL-3plus). The calibration was controlled by measuring literature quantum yield values of the dyes R590 and IR125. Additionally, upconversion quantum yield values were measured at another independent fluorescence system at the Molecular Foundry with good agreement between the two systems. Further experimental details are provided in the Supporting Information, Optical Characterization.

■ ASSOCIATED CONTENT

Supporting Information

The Supporting Information is available free of charge on the ACS Publications website at DOI: 10.1021/acs.nanolett.6b03683.

Synthesis procedures and supporting material characterization, transmission electron microscope images and size distribution analysis, excited state spectra and discussion on the upconversion and downshifting processes, time-dependent photoluminescence measurements of individual lanthanide energy levels, quantum yield measurements and methodology, surface quenching analysis of individual lanthanide energy levels, modeling of surface quenching assisted downshifting luminescence, and modeling of energy migration in ytterbium/erbium-doped crystals (PDF)

■ AUTHOR INFORMATION

Corresponding Author

*E-mail: paul.alivisatos@berkeley.edu.

Author Contributions

S.F. and A.P.A. conceived the project. S.F. synthesized the nanocrystals, conducted the spectroscopic measurements, measured the quantum yields, and performed the data analysis as well as the modeling with contributions from N.D.B., J.S., and E.M.C. All authors discussed the results and reviewed the manuscript.

Notes

The authors declare no competing financial interest.

■ ACKNOWLEDGMENTS

The authors thank Brent Koscher for synthesis advise and XRD measurements, Alex Powers for providing the analysis code for TEM images, and Xingchen Ye for valuable discussions. S.F. gratefully acknowledges the scholarship support from the German Research Foundation (DFG, agreement FI 2042/1-1). The work was supported by the Light-Material Interactions in Energy Conversion, an Energy Frontier Research Center funded by the U.S. Department of Energy, Office of Science, Office of Basic Energy Sciences, under Contract DE-AC02-05CH11231, part of the EFRC at Caltech under DE-SC0001293. Work at the Molecular Foundry was supported by the Office of Science, Office of Basic Energy Sciences, of the U.S. Department of Energy under Contract No. DE-AC02-05CH11231.

■ REFERENCES

(1) Zhang, R.; Lin, H.; Yu, Y.; Chen, D.; Xu, J.; Wang, Y. A New-Generation Color Converter for High-Power White LED: Transparent Ce^{3+}:YAG Phosphor-in-Glass. *Laser Photon. Rev/.* **2014**, *8*, 158−164.

(2) Pust, P.; Weiler, V.; Hecht, C.; Tücks, A.; Wochnik, A. S.; Henß, A.-K.; Wiechert, D.; Scheu, C.; Schmidt, P. J.; Schnick, W. Narrow-Band Red-Emitting $Sr[LiAl_3N_4]:Eu^{2+}$ as a next-Generation LED-Phosphor Material. *Nat. Mater.* **2014**, *13*, 891−896.

(3) Huang, X.; Han, S.; Huang, W.; Liu, X. Enhancing Solar Cell Efficiency: The Search for Luminescent Materials as Spectral Converters. *Chem. Soc. Rev.* **2013**, *42*, 173−201.

DOI: 10.1021/acs.nanolett.6b03683
Nano Lett. 2016, 16, 7241−7247

(4) Fischer, S.; Favilla, E.; Tonelli, M.; Goldschmidt, J. C. Record Efficient Upconverter Solar Cell Devices with Optimized Bifacial Silicon Solar Cells and Monocrystalline BaY_2F_8:30% Er^{3+} Upconverter. *Sol. Energy Mater. Sol. Cells* **2015**, *136*, 127−134.
(5) Goldschmidt, J. C.; Fischer, S. Upconversion for Photovoltaics - a Review of Materials, Devices and Concepts for Performance Enhancement. *Adv. Opt. Mater.* **2015**, *3*, 510−535.
(6) Eliseeva, S. V.; Bünzli, J.-C. G. Lanthanide Luminescence for Functional Materials and Bio-Sciences. *Chem. Soc. Rev.* **2010**, *39*, 189−227.
(7) Xue, X.; Wang, F.; Liu, X. Emerging Functional Nanomaterials for Therapeutics. *J. Mater. Chem.* **2011**, *21*, 13107−13127.
(8) Shen, J.; Zhao, L.; Han, G. Lanthanide-Doped Upconverting Luminescent Nanoparticle Platforms for Optical Imaging-Guided Drug Delivery and Therapy. *Adv. Drug Delivery Rev.* **2013**, *65*, 744−755.
(9) Fischer, S.; Johnson, N. J. J.; Pichaandi, J.; Goldschmidt, J. C.; Van Veggel, F. C. J. M. Upconverting Core-Shell Nanocrystals with High Quantum Yield under Low Irradiance: On the Role of Isotropic and Thick Shells. *J. Appl. Phys.* **2015**, *118*, 193105.
(10) Zhou, B.; Shi, B.; Jin, D.; Liu, X. Controlling Upconversion Nanocrystals for Emerging Applications. *Nat. Nanotechnol.* **2015**, *10*, 924−936.
(11) Meruga, J. M.; Baride, A.; Cross, W.; Kellar, J. J.; May, P. S. Red-Green-Blue Printing Using Luminescence-Upconversion Inks. *J. Mater. Chem. C* **2014**, *2*, 2221−2227.
(12) Wang, J.; Deng, R.; MacDonald, M. A.; Chen, B.; Yuan, J.; Wang, F.; Chi, D.; Hor, T. S. A.; Zhang, P.; Liu, G.; et al. Enhancing Multiphoton Upconversion through Energy Clustering at Sublattice Level. *Nat. Mater.* **2013**, *13*, 157−162.
(13) Chan, E. M.; Levy, E. S.; Cohen, B. E. Rationally Designed Energy Transfer in Upconverting Nanoparticles. *Adv. Mater.* **2015**, *27*, 5753−5761.
(14) Deng, R.; Qin, F.; Chen, R.; Huang, W.; Hong, M.; Liu, X. Temporal Full-Colour Tuning through Non-Steady-State Upconversion. *Nat. Nanotechnol.* **2015**, *10*, 237−242.
(15) Boyer, J.-C. C.; van Veggel, F. C. J. M. Absolute Quantum Yield Measurements of Colloidal $NaYF_4$: Er^{3+}, Yb^{3+} Upconverting Nanoparticles. *Nanoscale* **2010**, *2*, 1417−1419.
(16) Haase, M.; Schäfer, H. Upconverting Nanoparticles. *Angew. Chem., Int. Ed.* **2011**, *50*, 5808−5829.
(17) Pokhrel, M.; Kumar, G. a.; Sardar, D. K. Highly Efficient NIR to NIR and VIS Upconversion in Er^{3+} and Yb^{3+} Doped in M_2O_2S (M = Gd, La, Y). *J. Mater. Chem. A* **2013**, *1*, 11595−11606.
(18) Anderson, R. B.; Smith, S. J.; May, P. S.; Berry, M. T. Revisiting the NIR-to-Visible Upconversion Mechanism in β-$NaYF_4$:Yb^{3+}, Er^{3+}. *J. Phys. Chem. Lett.* **2014**, *5*, 36−42.
(19) Noculak, A.; Podhorodecki, A.; Pawlik, G.; Banski, M.; Misiewicz, J. Ion−ion Interactions in β-$NaGdF_4$:Yb^{3+}, Er^{3+} Nanocrystals − the Effect of Ion Concentration and Their Clustering. *Nanoscale* **2015**, *7*, 13784−13792.
(20) Hess, S.; Götz, M.; Davis, W. B.; Michel-Beyerle, M.-E. On the Apparently Anomalous Distance Dependence of Charge-Transfer Rates in 9-Amino-6-Chloro-2-Methoxyacridine-Modified DNA. *J. Am. Chem. Soc.* **2001**, *123*, 10046−10055.
(21) Gargas, D. J.; Chan, E. M.; Ostrowski, A. D.; Aloni, S.; Altoe, M. V. P.; Barnard, E. S.; Sanii, B.; Urban, J. J.; Milliron, D. J.; Cohen, B. E.; et al. Engineering Bright Sub-10-Nm Upconverting Nanocrystals for Single-Molecule Imaging. *Nat. Nanotechnol.* **2014**, *9*, 300−305.
(22) Riseberg, L. A.; Moos, H. W. Multiphonon Orbit-Lattice Relaxation of Excited States of Rare-Earth Ions in Crystals. *Phys. Rev.* **1968**, *174*, 429−438.
(23) Weber, M. J. Radiative and Multiphonon Relaxation of Rare-Earth Ions in Y_2O_3. *Phys. Rev.* **1968**, *171*, 283−291.
(24) Cao, T.; Yang, Y.; Gao, Y.; Zhou, J.; Li, Z.; Li, F. High-Quality Water-Soluble and Surface-Functionalized Upconversion Nanocrystals as Luminescent Probes for Bioimaging. *Biomaterials* **2011**, *32*, 2959−2968.
(25) Scatena, L. F. Water at Hydrophobic Surfaces: Weak Hydrogen Bonding and Strong Orientation Effects. *Science* **2001**, *292*, 908−912.
(26) Boyer, J. C.; Manseau, M. P.; Murray, J. I.; Van Veggel, F. C. J. M. Surface Modification of Upconverting $NaYF_4$ Nanoparticles with PEG-Phosphate Ligands for NIR (800 Nm) Biolabeling within the Biological Window. *Langmuir* **2010**, *26*, 1157−1164.
(27) Jacques, S. L. Optical Properties of Biological Tissues: A Review. *Phys. Med. Biol.* **2013**, *58*, R37−R61.
(28) Li, Z.; Zhang, Y. An Efficient and User-Friendly Method for the Synthesis of Hexagonal-Phase $NaYF_4$:Yb, Er/Tm Nanocrystals with Controllable Shape and Upconversion Fluorescence. *Nanotechnology* **2008**, *19*, 345606.
(29) Johnson, N. J. J.; Korinek, A.; Dong, C.; Van Veggel, F. C. J. M. Self-Focusing by Ostwald Ripening: A Strategy for Layer-by-Layer Epitaxial Growth on Upconverting Nanocrystals. *J. Am. Chem. Soc.* **2012**, *134*, 11068−11071.
(30) Li, X.; Shen, D.; Yang, J.; Yao, C.; Che, R.; Zhang, F.; Zhao, D. Successive Layer-by-Layer Strategy for Multi-Shell Epitaxial Growth: Shell Thickness and Doping Position Dependence in Upconverting Optical Properties. *Chem. Mater.* **2013**, *25*, 106−112.

DOI: 10.1021/acs.nanolett.6b03683
Nano Lett. 2016, 16, 7241−7247